Active and Passive Microrheology in Equilibrium and Nonequilibrium Systems

D. Mizuno,[†] D. A. Head,[‡] F. C. MacKintosh,[§] and C. F. Schmidt*[,||]

Organization for the Promotion of Advanced Research, Kyushu University, 812-0054 Fukuoka, Japan; Institute of Industrial Science, University of Tokyo, Meguro-ku, Tokyo 153-8505, Japan; Department of Physics and Astronomy, Vrije Universiteit, 1081HV Amsterdam, The Netherlands; and III. Physikalisches Institut, Fakultät für Physik, Georg-August-Universität, 37077 Göttingen, Germany

Received June 1, 2008; Revised Manuscript Received July 14, 2008

ABSTRACT: Quantitatively measuring the mechanical properties of soft matter over a wide range of length and time scales, especially if a sample is as complex as typical biological materials, remains challenging. Living cells present a further complication because forces are generated within these nonequilibrium materials that can change material properties. We have here developed high-bandwidth techniques for active one- and two-particle microrheology to tackle these issues. By combining active micromanipulation of probe particles with an optical trap with high-resolution tracking of thermal motions of the very same particles by laser interferometry, we can both measure the mechanical properties of and, at the same time, identify nonequilibrium forces in soft materials. In both simple liquids and equilibrium cytoskeletal actin networks, active microrheology (AMR) proves to be less noise sensitive than and offers extended bandwidth (0.1−100 kHz) compared to passive microrheology (PMR), which merely tracks thermal motions. We confirm high-frequency power-law dynamics in equilibrium actin networks with two-particle AMR and also discuss low-frequency local mechanical response near probe particles which shows up in one-particle AMR. The combination of AMR and PMR allowed us to quantify nonthermal force fluctuations in actin networks driven by myosin motor proteins. Our approach offers a new direct way to investigate the nonequilibrium dynamics of living materials.

Introduction

The material properties of soft condensed matter vary enormously across spatial and temporal scales, reflecting complex and hierarchical structures on micro- to mesoscopic scales. In the category "soft matter" fall synthetic colloids, polymer melts, and solutions which have wide industrial applications,[1] but also biological cells and tissues composed of mainly soft materials, such as biopolymers, gels, and lipid membranes. Biological materials typically present an even higher complexity in structure and dynamics than synthetic materials.[2,3] The fact that living systems are out of thermodynamic equilibrium can furthermore have profound effects on their mechanical properties. Understanding the mechanics on mesoscopic scales is a necessary step toward the systematic control of properties in both synthetic and biological soft matter.

Microrheology (MR) is a term for a number of techniques designed to probe small samples and to measure local viscous and elastic properties of materials by observing the motion of micrometer-sized probe particles.[4−8] Important advantages over conventional (macro)rheometry are that (i) viscoelasticity can be measured over a very wide frequency range since inertial effects are weak;[9,10] (ii) sample amounts can be as small as a femtoliter, i.e. one can measure in cells and tissues; and (iii) one can investigate how the material response is influenced by the probe particle size and surface properties.[11−14] For comparison, one can measure the correlated motions of two separated probe particles (two-particle MR), which is insensitive to modifications of the material in the immediate vicinity of the probe particles.[8,15−17] High bandwidth is necessary to capture complex dynamics in composite materials that often involve processes that occur on widely separated time scales. This has been achieved most successfully to date with passive microrheology (PMR),[4−8] which consists of merely monitoring thermal fluctuations of the probes. Passive methods, however, have still remained limited, particularly at high frequencies and for stiff materials. We employ here an active microrheology method (AMR) that directly measures the response of micron-sized particles to an oscillating optical trapping force.[18] The method provides a fully useable bandwidth of 0.1 Hz−100 kHz, considerably more than what has been achieved before by using external force application in other ways.[19−23] We demonstrate the capabilities of the method by quantitatively analyzing fundamental inertial effects in fluid flow using pure water as a model as well as high-frequency scaling laws in the elastic shear moduli G' and G'' of entangled filamentous actin solutions as model cytoskeletal systems.

A further fundamental challenge has to be overcome when studying nonequilibrium systems: One can, in principle, learn about internally generated nonequilibrium forces, e.g., in cells and tissues, by observing fluctuations as in PMR. To calculate forces and stresses from displacements, however, one needs to know the mechanical response characteristics of the material, which can be highly inhomogeneous and anisotropic. The response can be strongly affected by the forces themselves, such that it is not possible to use a control experiment on, e.g., a dead cell. The fluctuation measurement (PMR) can, in this case, not be used to calculate mechanical properties via the fluctuation−dissipation theorem (FDT) because fluctuations are no longer purely thermal. We introduce here an approach that solves this problem. It consists of combining in one experiment our new high-bandwidth AMR method with passive microrheology. We thereby practically simultaneously probe response and record fluctuations with exactly the same particle in exactly the same location of the sample. We demonstrate the method on "active gels", i.e., nonequilibrium actin networks driven by myosin motor proteins,[18] and show that it is possible to simultaneously determine shear elastic moduli and to analyze

* Corresponding author: Tel +49-551-397740, Fax +49-551-397720, e-mail cfs@physik3.gwdg.de.
[†] Kyushu University.
[‡] University of Tokyo.
[§] Vrije Universiteit.
[||] Georg-August-Universität.

10.1021/ma801218z CCC: $40.75
Published on Web 09/20/2008

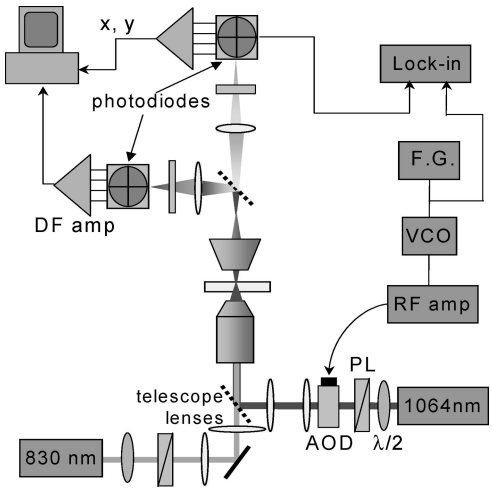

Figure 1. Schematic of the setup for both passive and active microrheology.

the low-frequency nonthermal fluctuations in the tensed networks.

Theoretical Foundations of Microrheology. *One-Particle Active Microrheology.* In AMR, the mechanical properties of the sample are determined from the response of imbedded, micron-sized probe particles to imposed forces. The probe particles are manipulated with a sinusoidally oscillated optical trap (drive laser), and their displacements are detected by laser interferometry with a second laser (probe laser), as shown in Figure 1 (details in Materials and Methods). The frequency-dependent displacement response $u(t) = u(\omega)e^{-i\omega t}$ of the probe particle is obtained as a complex quantity. Ignoring the influence of inertia, the (Langevin) equation of motion of a bead driven by an oscillatory force with frequency $f = \omega/2\pi$ is

$$k_2 u(t) + \int_{-\infty}^{t} \gamma(t - t)\dot{u}(t')\,dt' = k_1(Le^{-i\omega t} - u(t)) + \zeta(t) \tag{1}$$

where k_1 and k_2 refer to the trap stiffness of drive and probe laser, respectively, ζ is the random thermal force, L is the oscillation amplitude of the drive laser position, and $\gamma(t)$ is a friction function that reflects memory effects in the viscoelastic material. The Fourier transform of the ensemble or time average of eq 1 yields the frequency-dependent response of the probe particle, which we write as

$$u(\omega) = A(\omega)\,F(\omega) \tag{2}$$

Here, we introduced the Fourier transform $F(\omega) = 2\pi k_1 L\delta(\omega - \omega_0)$ of an apparent driving force $F(t) = k_1 Le^{-i\omega_0 t}$. [The actual force applied to the probe particle is $k_1(Le^{-i\omega t} - u(t))$. Since $u(t)$ depends on the material viscoelasticity which is not known during experiments, we define $k_1 Le^{-i\omega_0 t}$ as an apparent driving force.] An apparent complex response function $A(\omega)$ calculated as

$$A(\omega) = 1/[k_1 + k_2 - i\omega\gamma(\omega)] \tag{3}$$

includes the effects of both optical traps. The true response function $\alpha(\omega) = 1/[-i\omega\gamma(\omega)]$ that reflects only the rheology of the surrounding medium can be obtained as[24]

$$\alpha(\omega) = \frac{A(\omega)}{1 - k_t A(\omega)} \tag{4}$$

where $k_t = k_1 + k_2$. For a spherical probe in an incompressible, homogeneous viscoelastic medium with complex shear modulus $G(\omega) = G'(\omega) + iG''(\omega)$, this response function is given by the generalized Stokes relation[4,5]

$$\alpha(\omega) = \frac{1}{6\pi a G(\omega)} \tag{5}$$

where a is the radius of the probe particle.

One-Particle Passive Microrheology. For PMR, the oscillation of the drive laser is turned off in order to measure the unperturbed thermal and (if present) nonthermal fluctuations of a probe particle in the stationary optical trap. This can be done alternatingly with AMR in the same sample with the same beads. The time series data for bead positions are Fourier transformed to calculate the power spectral density (PSD) $C(\omega) \equiv \int_{-\infty}^{\infty}\langle u(t)u(0)\rangle e^{i\omega t}$ for both x and y directions. This quantity is, in equilibrium, related to the imaginary part $A''(\omega)$ of the complex response function $A(\omega) = A'(\omega) + iA''(\omega)$ via the fluctuation−dissipation theorem (FDT):[25]

$$C(\omega) = \frac{2k_B T}{\omega} A''(\omega) \tag{6}$$

Provided that $A''(\omega)$ is known over a large enough range of frequency, the real part of the response function $A'(\omega)$ can be obtained from a Kramers−Kronig integral:[6,25,26]

$$A'(\omega) = \frac{2}{\pi} P \int_0^{\infty} \frac{\xi A''(\xi)}{\xi^2 - \omega^2}\,d\xi \tag{7}$$

where P denotes a principal-value integral. From the apparent response $A(\omega)$, which is influenced by the optical trap, we can then, with eq 4, obtain $\alpha(\omega)$ which describes the pure material response.

Two-Particle Active Microrheology. In two-particle AMR, the mechanical properties of the sample are determined from the response of one particle at position $(u_x^{(1)},u_y^{(1)})$ to an oscillating force applied to a second particle at position $(u_x^{(2)},u_y^{(2)})$. The superscripts refer to the two different particles. The presence of probe particles breaks the symmetry of the system, which would otherwise exist in an isotropic material. The coordinate system is chosen such that x is parallel (∥) and y is perpendicular (⊥) to the line connecting the particle centers. For an isotropic, homogeneous medium, two independent parameters $\alpha_{\parallel}(\omega)$ and $\alpha_{\perp}(\omega)$ (corresponding to the response to forces in x and y directions) determine the full linear response. In Fourier space, it is written as[15,17]

$$\begin{aligned} u_x^{(1)}(\omega) &= \alpha_{\parallel}(\omega)F_x^{(2)}(\omega) \\ u_y^{(1)}(\omega) &= \alpha_{\perp}(\omega)F_y^{(2)}(\omega) \end{aligned} \tag{8}$$

and similarly for exchanged indices 1 and 2.

When the particles are confined by the optical traps, which is necessary in viscous media, the potential wells created by the trapping and detection lasers also affect the response, generating the directly measured (apparent) response functions A, which differ from the intrinsic rheological response functions α of the material. For a pair of particles, their displacements $u^{(i)}$ can be expressed in terms of the single-particle response functions $\alpha^{(i)}$, the mutual or two-particle response functions $\alpha_{\parallel,\perp}$, the trapping forces $-k^{(i)}u^{(i)}$, and the applied forces $F^{(i)}$, leading to[19,24]

$$\begin{aligned} u_x^{(1)} &= \alpha^{(1)}[F_x^{(1)} - k^{(1)}u_x^{(1)}] + \alpha_{\parallel}[F_x^{(2)} - k^{(2)}u_x^{(2)}] \\ u_x^{(2)} &= \alpha^{(2)}[F_x^{(2)} - k^{(2)}u_x^{(2)}] + \alpha_{\parallel}[F_x^{(1)} - k^{(1)}u_x^{(1)}] \end{aligned} \tag{9}$$

and similarly exchanging $x \rightarrow y$ and/or $\parallel \rightarrow \perp$. When a force $F^{(1)}$ is applied to particle 1 in addition to the trapping force $-k^{(1)}u^{(1)}$, the response of particle 2 defines the apparent response functions $A_{\parallel,\perp}^{(2,1)}$ and $A_{\perp}^{(2,1)}$ by $u_x^{(2)}(\omega) = A_{\parallel,\perp}^{(2,1)}(\omega)F_x^{(1)}(\omega)$ and $u_y^{(2)}(\omega)$

$= A_{\perp}^{(2,1)} F_y^{(1)}(\omega)$. In the case of two-particle AMR, a sinusoidal displacement $u_0(t) = Le^{-i\omega_0 t}$ of the position of trap 1 results in a net force of $k^{(1)}[u_0 - u^{(1)}]$ on particle 1, which amounts to an apparent applied force $F_x^{(1)} = F_{app} = k^{(1)}u_0(t)$. From the resulting displacement $u_x^{(2)}$, we determine the response function $A_{\parallel}^{(2,1)}$, which can be expressed as[24]

$$A_{\parallel}^{(2,1)} = \frac{\alpha_{\parallel}}{(1 + k^{(1)}\alpha^{(1)})(1 + k^{(2)}\alpha^{(2)}) - k^{(1)}k^{(2)}\alpha_{\parallel}^{\,2}} \tag{10}$$

Again, there is a similar expression for exchanging $\parallel \rightarrow \perp$. From this response function which can be measured directly, the rheological response function of the medium can be calculated as[24]

$$\alpha_{\parallel} = \frac{A_{\parallel}^{(2,1)}}{(1 - k^{(1)}A^{(1)})(1 - k^{(2)}A^{(2)}) - k^{(1)}k^{(2)}A_{\parallel}^{\,2}} \tag{11}$$

provided that the trap strengths $k^{(i)}$ and the apparent one-particle response functions $A^{(i)}$ are also measured.

Two-Particle Passive Microrheology. For the passive measurements, the oscillation of the drive laser is turned off in order to measure the unperturbed thermal fluctuations of both probe particles in the two stationary optical traps. We calculate the cross-correlation functions[16]

$$C_{\parallel}(\omega) = \int_{-\infty}^{\infty} \langle u_x^{(1)}(t) u_x^{(2)}(0)\rangle e^{i\omega t} \tag{12a}$$

and

$$C_{\perp}(\omega) = \int_{-\infty}^{\infty} \langle u_x^{(1)}(t) u_x^{(2)}(0)\rangle e^{i\omega t} \tag{12b}$$

The FDT relates these to the response functions $A_{\parallel,\perp}(\omega)$, provided that the system is in equilibrium:

$$C_{\parallel,\perp}(\omega) = \frac{2k_B T}{\omega} A''_{\parallel,\perp}(\omega) \tag{13}$$

Here, we have suppressed the superscripts denoting particles 1 and 2, since $A^{(2,1)} = A^{(1,2)}$ for both parallel and perpendicular motion. This is justified by the symmetry in eq 10 as well as from eqs 12a and 13, since the correlation functions $\langle u^{(1)}(t)\ u^{(2)}(0)\rangle$ must be symmetric under time translation and reversal. From the imaginary parts of the response functions $A_{\parallel,\perp}(\omega)$, the real parts are obtained using a Kramers−Kronig relation as above. Then the rheological response functions $\alpha_{\parallel,\perp}(\omega)$ are obtained using eq 11. For an incompressible continuum with shear modulus $G(\omega)$, the two-particle response functions are given by the generalized Oseen tensor:[15,17]

$$\alpha_{\parallel} = \frac{1}{4\pi G(\omega) r} \quad \text{and} \quad \alpha_{\perp} = \frac{1}{8\pi G(\omega) r} \tag{14}$$

where r is the distance between the two particles.

Results

One-Particle Microrheology in Water. First and as a control, both active and passive one-particle MR were carried out in water using exactly the same probe particle. Figure 2a shows A' and A'' as a function of frequency with fits by eq 3. In this equilibrium situation, where fluctuations are purely thermal, active and passive MR agree within an experimental error of ∼10%. When a probe particle is optically trapped, thermal fluctuations below the corner frequency $\omega_c = k_t/\gamma$ ($\gamma = 6\pi\eta a$, particle radius a, fluid viscosity η, total trap stiffness $k_t = k_1 + k_2 = 1.06 \times 10^{-4}$ N/m) are suppressed. Noise from mechanical vibrations, laser pointing fluctuations, or fluctuations in the AOD deflection angle then adds to the PSD of the actual displacement fluctuations in a biased way, such that the response functions obtained with PMR are overestimated, especially below the corner frequency (Figure 2a).

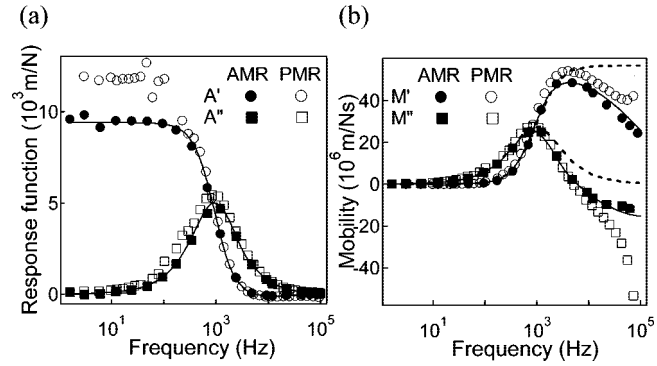

Figure 2. One-particle response functions in water. (a) Real (circles) and imaginary part (squares) of the complex response function (probe particle radius $a = 1.05$ μm) measured with AMR (filled symbols) and PMR (open symbols). Solid lines are the theoretical curves obtained without using free parameters. Low-frequency noise causes 10−20% ambiguity in PMR. (b) Same spectra shown as the mobility $M \equiv -i\omega A$. At high frequencies, a significant difference between AMR and PMR was observed because of the finite frequency cutoff in the Kramers−Kronig integral in PMR. Broken lines are the data without inertia taken into account. Model curves taking into account inertia (solid lines) agree well with the AMR data.

Plotting the apparent mobility $M(\omega) = M' + iM'' = -i\omega A(\omega)$ (M'' is negative in this notation) emphasizes the behavior at high frequencies (Figure 2b). The discrepancy between active and passive MR at frequencies higher than 10 kHz is caused by the finite frequency cutoff in the Kramers−Kronig integral in eq 7. The AMR data are not affected by this effect, but also do not agree well with the theoretical curves (dashed lines in Figure 2b) given by

$$M = -i\omega A = \frac{-i\omega}{k_t - i\omega\gamma} \tag{15}$$

The reason for the discrepancy is that eq 15 is valid for slow motions of a probe particle when inertia can be neglected, but it is not valid at high frequencies. Inertia of the probe particle and the surrounding fluid which moves with it must be taken into account to obtain the mobility at high frequencies. The friction between rigid particle and fluid also starts to depend on the particle's past motion for short times (∼10^{-6} s). Taking these two effects into account, the mobility μ can be calculated as[9,10]

$$\mu = -i\omega\alpha = \frac{-i\omega}{k_t - 6\pi\eta a(1 + a/\delta)i\omega - \omega^2(3\pi\rho_0 a^2\delta + 2\pi\rho_0 a^3/3 + 4\pi\rho a^3/3)} \tag{16}$$

where ρ_0 and ρ are the densities of solvent and probe particle and $\delta = (\eta/\rho\pi f)^{1/2}$ is the viscous penetration depth describing the exponential decrease of the fluid's velocity field away from the oscillating sphere. As shown in Figure 2b, eq 16 describes the AMR data well using only one free fit parameter k_t, which indicates the importance of these effects.

Two-Particle Microrheology in Water. Two-particle PMR and AMR in water agreed to within experimental error below 40 kHz, as shown in Figure 3 for two probe particle pairs separated by $r = 11.3$ μm and by $r = 10.5$ μm. A plot of two-particle mobilities $M_{\parallel,\perp} \equiv -i\omega A_{\parallel,\perp}$ again provides a better view on differences at high frequencies (Figure 3b,d). The dashed

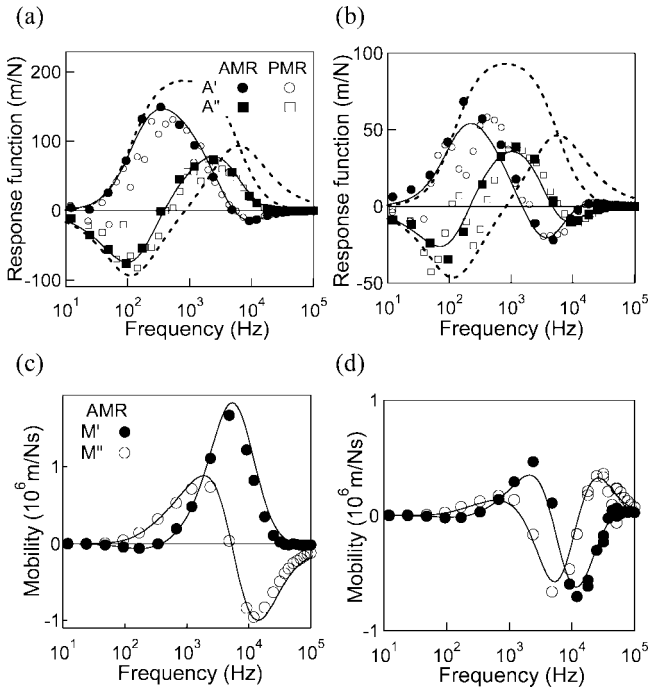

Figure 3. Two-particle response functions in water. (a) Real (circles) and imaginary part (squares) of the complex parallel response function $A_{12\parallel}(\omega)$ (probe particle radius $a = 1.05$ μm, separation $r = 11.3$ μm) measured with AMR (filled symbols) and PMR (open symbols). Broken lines are the theoretical curves from eq 10. Solid lines are theory curves including inertial effects as given in eqs 17 and 18a. Since trap stiffnesses (parallel: $k_1 = 4 \times 10^{-4}$ N/m, $k_2 = 7.7 \times 10^{-6}$ N/m; perpendicular: $k_1 = 3.7 \times 10^{-4}$ N/m, $k_2 = 7.9 \times 10^{-6}$ N/m) are obtained from independent one-particle MR measurement, there are no adjustable parameters. (b) Same for the perpendicular response function $A_{12\perp}(\omega)$ for a second bead pair (separation $r = 10.5$ μm) measured in water. (c, d) The frequency dependence characteristic of the inertial response can be seen in the mobility spectra (c for parallel and d for perpendicular) defined as $M \equiv -i\omega A$; active MR agrees well with theory (eq 21) in the whole frequency range observed.

lines in Figure 3a represent the expected response functions (eq 10) without the contribution of inertia. Inertia has a stronger effect on two-particle MR than on one-particle MR because stress needs to propagate over the distance between the two particles while in one-particle MR the relevant length scale is the radius of the probe bead. Inertial propagation of stress in a viscous medium is diffusive, i.e., the time required for stress propagation grows with the square of the distance. Taking inertia into account results in consistency with both theory and prior results obtained by PMR.[27,28]

The response function for a general viscoelastic medium within the Oseen approximation ($r \gg a$) was obtained as[29−31]

$$\alpha_{\parallel} = \frac{1}{4\pi G(\omega) r}\chi_{\parallel}(r\sqrt{\kappa}), \quad \alpha_{\perp} = \frac{1}{8\pi G(\omega) r}\chi_{\perp}(r\sqrt{\kappa}) \qquad (17)$$

where r is the separation distance between the two particles and $\kappa = \rho\omega^2/G(\omega)$ is a complex quantity, the magnitude of which is the inverse square of the viscoelastic penetration depth, and the correction factors are

$$\chi_{\parallel}(x) = \frac{2}{x^2}((1 - ix)e^{ix} - 1) \qquad (18a)$$

$$\chi_{\perp}(x) = \frac{2}{x^2}(1 + (x^2 - 1 + ix)e^{ix}) \qquad (18b)$$

The solid lines in Figure 3 are the theoretical curves calculated by combining eq 17 with eq 10. Agreement with the active MR

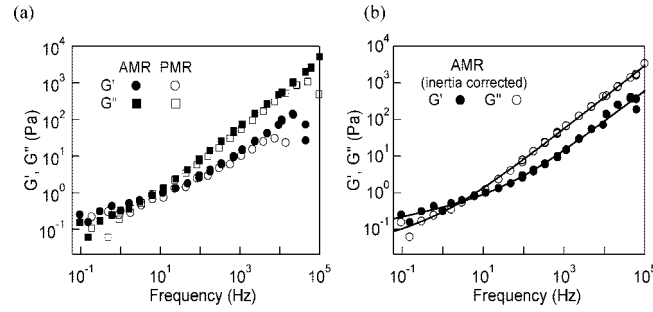

Figure 4. One-particle MR (probe radius $a = 1.28$ μm) in an entangled actin solution (1 mg/mL concentration). (a) Real part (circles) and imaginary part (squares) of the complex shear modulus obtained by AMR (filled symbols) and PMR (open symbols). Active and passive MR deviates at frequencies higher than several kHz because of the Kramers−Kronig integral in passive MR. (b) Complex shear modulus measured with AMR after correcting for inertia and the contribution of the viscosity of solvent $-i\omega\eta_s$. Approximate power law behavior is observed. Solid lines are the fit with eq 19.

data is good without adjustable parameters. The trap stiffnesses k_1, k_2, and the other necessary parameters were independently determined as described in the Methods section.

One-Particle Microrheology in Actin. After having tested PMR and AMR in a viscous liquid, we further applied the method to entangled F-actin solutions. Shear moduli G' and G'' measured with one-particle active and passive MR are shown in Figure 4a. Here we again observed that AMR performs better at high frequencies. PMR suffers from the finite frequency cutoff in the Kramers−Kronig integral at frequencies higher than ~10 kHz when fluctuations are recorded with 100 kHz bandwidth. Since there is no such artifact in the AMR data, fluid inertial effects were quantitatively detected in G' and G''. Therefore, it is possible to obtain the shear moduli up to higher frequencies. The expression for the mobility of a probe particle embedded in a viscoelastic material can be obtained by substituting the frequency-dependent complex viscosity $\eta(\omega) = -(G' + iG'')/i\omega$ for η in eq 16. The solution of the resulting equation can be multivalued. Only a single stable solution is found, however, if the initial estimate for $G(\omega)$ is in the physically possible range. By solving the resulting equation numerically, we obtained an inertia-corrected $G(\omega)$ over the full frequency range measured. After subtracting the contribution from the solvent viscosity, $-i\omega\eta_s$ (η_s: solvent viscosity), the resulting complex shear modulus for F-actin is plotted in Figure 4b.

The (apparent) shear modulus of the actin solutions measured with one-particle MR can be approximately described as a sum of two power laws:

$$G(\omega) = C_1(-i\omega)^a + C_2(-i\omega)^b \qquad (19)$$

The solid lines in Figure 4b are fits to eq 19 with parameters $C_1 = 0.033$, $a = 0.84$, $C_2 = 0.26$, and $b = 0.23$. Similar behavior of actin solutions was observed in prior studies.[5,6,32] Power-law behavior at high frequencies is ubiquitous for polymer networks and well understood in terms of single-filament dynamics on scales below that of an effective entanglement length.[26,33,34] With AMR, not only G'' but also G' can be followed well into the high-frequency power-law regime, which had not been possible in earlier PMR experiments.[6] The transition to a different power law at low frequencies could be the gradual emergence of an elastic plateau, but comparison with two-particle results (see below) shows that it is likely that this transition reflects a local effect (described in detail in ref 14), found only in the one-particle response, that does not reflect the bulk behavior of the embedding medium.

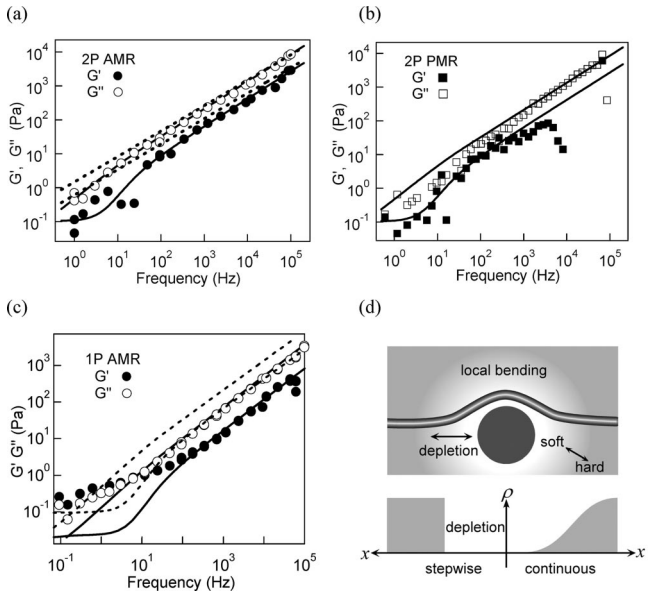

Figure 5. Two-particle MR (probe radius $a = 1.28\ \mu$m, distance $r = 12.1\ \mu$m) in an entangled actin solution (1 mg/mL concentration). (a) Real (filled circles) and imaginary part (open circles) of the complex shear modulus measured with AMR. Broken lines are the theoretically predicted asymptotic behavior $G(\omega) \sim 1.6(-i\omega/2\pi)^{3/4}$ for an actin solution. Solid lines are theory including additional relaxation by end retraction,[33] parameters exactly as in ref 33 with contour length equal to the persistence length. (b) Real (filled squares) and imaginary part (open squares) of the complex shear modulus measured with PMR. Bandwidth is limited to ~1 kHz because inertia cannot be corrected. Solid lines are the same theoretical curve as those shown in (a). Low-frequency noise causes G'' to be underestimated. (c) Comparison of bulk shear modulus (broken lines) and one-particle MR (G': filled circles; G'': open circles). Solid lines are the theoretical curve for the continuous depletion model (ζ equal to probe radius). (d) Schematic illustration of the continuous depletion layer and local deformation of an actin filament (upper) and the concentration profile of actin for each depletion model (lower).

Two-Particle Microrheology in Actin. Figure 5a,b shows the complex shear modulus, G' and G'', measured with two-particle active and passive MR. The influence of the two optical traps can be taken into account using eq 11. Having already confirmed in the previous section that one-particle active and passive MR give quantitative agreement at low frequencies where the effects of the optical trap are most relevant, we used $A^{(1)}$ and $A^{(2)}$ obtained by one-particle PMR to insert into eq 11. We furthermore took solvent inertia into account by numerically solving eqs 17 and 18a. The resulting curves for G' and G'' are shown in Figure 5a for AMR and Figure 5b for PMR. Both G' and G'' clearly show the high-frequency power-law behavior in the AMR data (Figure 5a), while for PMR data the high-frequency regime of G' is cut off by the Kramers−Kronig integral, and clear high-frequency power-law behavior is not seen (Figure 5b).

The microscopic origin of the mechanical properties of actin networks are the relaxations of the thermally undulating semiflexible actin filaments. For solutions in the limit of high molecular weight, these relaxations in a viscous embedding medium lead to power-law behavior of the shear modulus with an exponent 3/4 at high frequencies.[26,34] Experimentally, it has been reported[18,35,36] that the high-frequency response of "cross-linked" actin networks shows good quantitative agreement with the theoretical predictions $G(\omega) = 1.6(-i\omega/2\pi)^{3/4}$ (for 1 mg/mL actin[26,34]) plotted as a dashed line in Figure 5a. "Non-cross-linked" solutions of finite-length semiflexible polymers, which we have studied here, exhibit an additional mode of relaxation associated with retraction of their free ends under shear or extensional flow.[33,37−39] This results in a reduced shear modulus and a deviation from the pure 3/4 power-law scaling shown as a dashed line in Figure 5a. This has been already suggested in prior two-particle PMR results,[35] and we also confirm it here more clearly by correcting for the influence of fluid inertia with AMR. The theoretical curves in Figure 5a,b were calculated according to refs 33 and 39 using the appropriate parameters for an entangled actin solution at a concentration of 1 mg/mL and (estimated) filament length equal to the persistence length. Thus, the AMR data agree well with theoretical predictions without adjustable parameters in the whole range of frequencies measured.

There remains a small systematic discrepancy between AMR and PMR two-particle data. The shear modulus measured with PMR shown in Figure 5b is smaller than both the AMR results and the theoretical curve. This might be due to additional nonthermal fluctuations caused by slow nonequilibrium processes, such as polymerization and depolymerization of actin[40] or by mechanical noise in the setup.

Local Mechanical Response in Equilibrium Actin Networks. Having concluded that two-particle AMR accurately measures the bulk viscoelasticity of entangled actin solutions, we now discuss the local elastic response manifest as the difference between the one-particle MR result and the bulk shear modulus or two-particle MR result (Figure 5c). Because of steric exclusion, which is expected to have a rather long-range effect given the semiflexibility of F-actin filaments, it has been suggested[33,41,42] that there exists a layer of micrometer thickness around the probe particles that is partially depleted of actin. This effect has been tested experimentally in DNA and actin solutions and modeled approximately by assuming a completely depleted shell around the probe particles.[14,17,43] Instead of such a discontinuous concentration profile around the probe, we here use another model of ref 17 with a corona consisting of a continuously increasing actin concentration. The model considers a discrete series of contiguous depletion shells around the probe particle. The strain field is calculated using stress and displacement continuity at the shell boundaries, and then the limit of infinitesimal thickness for each layer is taken. Since we do not precisely know the density gradient for actin filaments near a sphere, we use the concentration profile that has been calculated for semidilute polymers near a flat wall[17,44,45]

$$\rho(x) = \rho_0 \tanh^2(x/\xi) \tag{20}$$

where ρ_0 is the bulk concentration in units of contour length per unit volume (3.9×10^{13} m^{-2}). This approach is still an approximation that neglects the fact that the depletion depth is roughly on the order of the mesh size and the persistence length of the actin filaments (all micrometers) which makes a continuum approximation become marginal. Knowing the bulk shear modulus $G(\rho,\omega)$ of actin solutions as a function of actin concentration (based on the model[33,39] which we tested here as shown in Figure, 5), we numerically calculated the one-particle response function within the continuous depletion model and obtained the apparent shear modulus from the Stokes−Einstein relation (eq 5). The solid lines in Figure 5c show the model curves with one adjustable parameter, the characteristic thickness of the depletion layer ξ. The high-frequency power law behavior shows good agreement for both G' and G'' between one-particle MR and the numerical calculation with ξ equal to the probe radius. This approach provides a better explanation of the observed one-particle response (Figure 5d), especially of the elastic part of the response that tends to be neglected by a purely viscous depletion shell.

The continuous shell model we used here also assumes that the medium is incompressible. Strong coupling between the

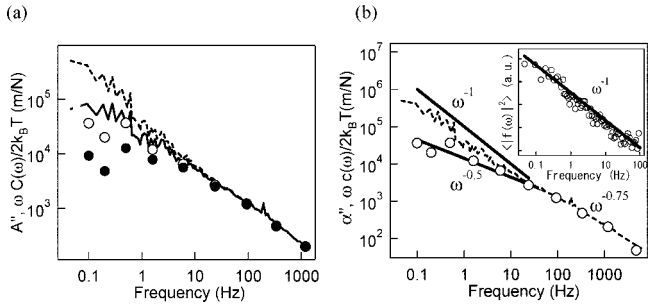

Figure 6. (a) Imaginary part of one-particle response functions in a nonequilibrium system. The apparent response function A'' measured with AMR (filled circles) and PMR (solid line). The response function α'' after eliminating the effect of the optical trap using eq 21, measured with AMR (open circles) and PMR (broken line). Nonequilibrium fluctuations show as disagreement between AMR and PMR (arrow) at frequencies <10 Hz. (b) Trap-corrected response functions α'' (open circles) and α''_{app} (broken line) measured with AMR and PMR, respectively, which show distinct power law behaviors. Inset shows the motor-generated force spectrum calculated by comparing AMR and PMR.

solvent and the polymer network guarantees incompressible mechanical response at large distances and/or short time scales.[6,26] It should be noted, however, that slow and local deformation of filaments can decouple from the solvent motion, violating incompressibility. This could be one reason for the disagreement between the numerical calculation and experimental data in Figure 5c at low frequencies. There is a further effect that probably explains the deviations of the one-particle response from the bulk results, namely the effect of local bending of filaments (Figure 5d). A systematic study of this effect will be published elsewhere.[14]

Detection of Nonthermal Forces in an Out-of-Equilibrium Actin−Myosin Network. In systems out of thermodynamic equilibrium, the fluctuation−dissipation theorem need not be valid since the displacement fluctuations of probe particles are driven not only by thermal but also by nonthermal forces. Combining AMR and PMR and evaluating the difference between the results, using the same beads in the same samples, is thus a convenient and accurate way to test for nonequilibrium behavior of a system and to quantify the nonthermal fluctuations by calculating $\langle|u(\omega)^2\rangle_{\text{nonthermal}} = C(\omega) - 2k_BT\alpha''/\omega$, where α'' is the imaginary part of the response function measured by AMR. We have reported nonequilibrium fluctuations of probe particles in a strongly cross-linked actin network driven by myosin motor proteins in a previous study.[18] Here we focus on the method and demonstrate the principle of the approach in more detail on a similar system, consisting of an actin/myosin gel that was not cross-linked in addition to the transient cross-linking provided by the myosin motors themselves.

Figure 6a shows one-particle active and passive MR data. We observed a clear difference between spectra measured by AMR and PMR at frequencies lower than ~10 Hz and good agreement at frequencies above ~10 Hz. Shown are the response functions measured by AMR with (α'') and without (A'') correction for the influence of the optical trap using eq 4. PMR, in this out-of-equilibrium sample, reports the totality of fluctuations, thermal and motor-generated, and because of that the true response function cannot be determined via FDT with eq 6. To bring the PMR results in a form that can be compared with the AMR results, we calculate the normalized power spectral density as $\omega C(\omega)/2k_BT$. In the presence of the optical trap, the total observed particle fluctuations $C(\omega)$ can then be expressed as the sum of thermal and nonthermal fluctuations as

$$C(\omega) = \langle|u(\omega)|^2\rangle_{\text{thermal}} + \langle|u(\omega)|^2\rangle_{\text{nonthermal}} = \frac{2k_BTA''}{\omega} + |A(\omega)|^2\langle|f(\omega)|^2\rangle \quad (21)$$

where $f(\omega)$ denotes the Fourier transform of the motor-generated nonequilibrium forces acting on the probe particle. Using eq 4, we obtain the trap-corrected normalized power spectral density $c(\omega)$ measured with PMR, which is determined from

$$C(\omega) = \frac{1}{(1 + k\alpha)(1 + k\alpha^*)}\left\{\frac{2k_BT\alpha''}{\omega} + |\alpha(\omega)|^2\langle|f(\omega)|^2\rangle\right\} \equiv \frac{c(\omega)}{(1 + k\alpha)(1 + k\alpha^*)} \quad (22)$$

This last step in the data processing is necessary because, due to the softness of the non-cross-linked actin/myosin gel, the optical trap had a non-negligible effect on the response functions (Figure 6a) (whereas in the strongly cross-linked gels studied previously the trap effect could be ignored[18]). The combination of AMR and PMR is therefore not just necessary to distinguish nonequilibrium from thermal fluctuations, but is also indispensable to correct for the influence of the optical trap in the PMR data.

In Figure 6b, we compare the trap-corrected AMR and PMR results. Agreement of AMR and PMR above 10 Hz implies that the motor-generated nonthermal fluctuations are negligible in this regime; both methods give the actual response of the material. At high frequencies, we observe power-law behavior typical for a semiflexible polymer network $\alpha''(\omega) \sim \omega^{-0.75}$. At frequencies just below 10 Hz the actual response function measured with AMR displays a smaller log−log slope and has approximately a power-law form of $\alpha''(\omega) \sim \omega^{-0.5}$. This is exactly what is expected from a network with internal motor-generated tension as reported before.[18] At frequencies below 10 Hz, there is also a clear difference between (trap-corrected) AMR and PMR results. This is due to the motor-generated nonthermal fluctuations. The apparent response function measured by PMR has approximately a power-law slope of $\alpha''(\omega) \sim \omega^{-1}$ over a rather wide frequency range. It is interesting to note, as an aside, that the power-law slope in the response function with an exponent of -1 corresponds to a power-law slope with exponent -2 in the power spectral density of the displacement fluctuations. This is by coincidence exactly what is seen for diffusion in a purely viscous medium in equilibrium. Displacement spectra with slope of -2 at such low frequencies have also been observed in cells,[46,47] and it is tempting to interpret these as the result of free thermal diffusion. This potential error is avoided by comparing PMR with AMR where it is obvious that the network has clearly viscoelastic response and that the displacement fluctuations are at these frequencies dominated by nonequilibrium fluctuations. The inset of Figure 6b shows the spectrum of force fluctuations, calculated from the comparison of AMR and PMR using eq 22. The spectrum of the force fluctuations in the non-cross-linked actin−myosin networks scaled approximately as $\langle|f(\omega)|^2\rangle \sim \omega^{-1}$. This is different from what had been found in a cross-linked active gel where $\langle|f(\omega)|^2\rangle \sim \omega^{-2}$. A possible explanation for the latter behavior was the slow buildup of tension followed by sudden release caused by the sudden detachment of myosin multimers from the actin filaments.[18,48] Here, on the other hand, in non-cross-linked active gels,[49] it is likely that several myosin minifilaments work cooperatively and that the restoring forces from the network are smaller. Therefore, both the development and the release of tension should become more gradual. An explanation beyond this qualitative argument will have to await further experiments.

Conclusions

We have performed active and passive MR using exactly the same probe particle, both in water and in an entangled F-actin solution which served as a model for the cell cytoskeleton. By comparing results, we have demonstrated the advantages of the active variant of high-bandwidth microrheology. Active MR allowed us to quantitatively measure both real and imaginary parts of the shear modulus up to 100 kHz and to quantitatively explore fluid inertial effects. At low frequencies, where PMR is limited by noise, AMR gave more precise results with better signal-to-noise ratio than PMR. The application of AMR to the entangled actin network extended earlier results and now clearly confirms that the frequency dependence of the complex shear modulus is well described by theoretical models. In particular, two-particle AMR agreed well with theory. One-particle active MR, in contrast, turned out to be very sensitive to local structural and dynamic inhomogeneities caused by the probe particle itself. While in equilibrium samples AMR and PMR gave the same results in the frequency range where both are reliable, in nonequilibrium systems, the combination of both methods provides a unique and very accurate way to quantify the nonthermal fluctuations and to calculate the spectrum of the forces driving the system out of equilibrium.

Materials and Methods

Experimental Setup. The experimental setup, shown schematically in Figure 1, consisted of two optical traps made with lasers of two different wavelengths.[16] In AMR, one of the lasers was operated at higher power (drive laser, $\lambda = 1064$ nm, Nd:YVO_4, Compass, Inc., Santa Clara, CA) and was deflected by an acousto-optic deflector (AOD, model DTD 276HB6, IntraAction, Corp., Bellwood, IL). The AOD was driven by a voltage-controlled oscillator (VCO, model AA.DRF. 40, AA Sa, Orsay, France). By sinusoidally modulating the output frequency of the VCO, the deflection angle of the AOD (and the location of the laser focus in the sample plane) was oscillated. The other optical trap ($\lambda = 830$ nm, IQ1C140/6017, Laser 2000, BeNeLux C. V., Vinkeveen, Netherlands) was stationary and was used to sensitively detect the position of either the same probe particle (one-particle AMR) or a different second probe particle (two-particle AMR). The technique used in this study for precise position detection was back-focal-plane laser interferometry.[50] The angular deflection of the probe laser due to the displacement of the probe particle was detected with a quadrant photodiode (QPD, SPOT9D, OSI optoelectronics AS, Horten, Norway), and the output signal from the QPD was measured with a lock-in amplifier (model SR830, Stanford Research Systems, Inc., Sunnyvale, CA). The lock-in amplifier was provided with a reference signal derived from the VCO.

For PMR, the oscillation of the drive laser was turned off and the thermal motions of probe particles were detected. The output signal from the QPD was digitized at 195 kHz with an A/D board (AD16 board on a ChicoPlus PC-card, Innovative Integration, Simi Valley, CA) and recorded with a PC. After passing through the sample, the probe laser and drive laser were collimated with the high-numerical-aperture condenser lens (1.4 NA) and separated again with a polarizing beam splitter, followed by a laser line filter for the respective wavelength. Then an image of the back-focal plane of the condenser was projected onto two independent QPDs.

Calibration. The particle position $u(t)$ and the applied trapping force were obtained from the linear relation to the output voltage of the QPDs. In order to obtain the calibration factor for the particle position, $Cal \equiv u(t)/V(t)$, and the stiffness k of the optical trap, power spectral densities of probe particles were recorded in water and fitted with a Lorentzian in the form of[51]

$$C(\omega) = \frac{2k_B T}{\gamma(\omega_c^2 + \omega^2)} \tag{23}$$

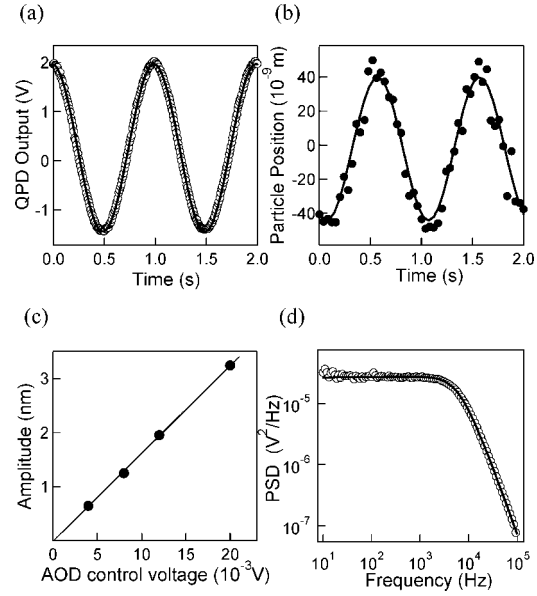

Figure 7. Direct calibration by oscillating a probe particle (a−c) and conventional calibration using the PSD of thermal fluctuations. (a) The output of the probe laser overlapping with the oscillating drive laser. (b) Position of the trapped particle obtained from video images. (c) Linear relation between QPD output and particle displacement. The calibration factor obtained with this method was 25.4×10^{-9} m/V. (d) Power spectrum of the same particle in water without oscillation. The calibration factor obtained by fitting with eq 22 was 28×10^{-9} m/V.

Here, $\omega_c = k/\gamma$ is the corner frequency of the Lorentzian, and the friction coefficient γ is given by the Stokes formula $\gamma = 6\pi\eta a$, where a is the particle radius and η is the viscosity of fluid. Knowing the bead diameter, the solvent viscosity and temperature, we obtain Cal and k.

The derivation of the calibration factor Cal using eq 23 is based on the fluctuation−dissipation theorem (FDT). In order to, alternatively, directly obtain this calibration factor, a colloidal particle attached to a coverslip was moved by a known distance with a piezo-driven stage, and the deflection of the detection laser by the particle was measured. This method neglects that the calibration factor generally depends on the distance of the trapped particle from the bottom of the sample chamber because of spherical aberrations occurring at the glass−water interface in the sample chamber when using an oil immersion objective.[52] Close to the coverslip, interference by multiple reflections between the probe particle and the glass surface can also influence the deflection pattern at the back focal plane.[53] In this study, we trapped a probe particle ($a = 1.28$ μm) with the drive laser at the same height (20 μm from the bottom surface) as was used in the rest of the experiments and oscillated the particle slowly (∼1 Hz) with the AOD so that the probe particle completely followed the focus of driving laser. The sinusoidal response of the output of the QPD for the probe laser was recorded as shown in Figure 7a. In order to obtain the amplitude of the laser oscillations L, the oscillatory motion of the same bead was video recorded (IMAQ, image capture board PCI 1405, National Instruments), and the position of the center of mass of the particle was tracked as shown in Figure 7b. We found a calibration factor of 2.53×10^{-8} m/V by plotting the amplitude of the displacement (nm) versus output voltage (V), as shown in Figure 7c. At the same time, as shown in Figure 7d, $\langle |V(\omega)|^2 \rangle$ for the probe laser was measured under exactly the same conditions, except turning off the oscillation of the drive laser. From fitting with eq 23, the calibration factor was obtained as 2.8×10^{-8} m/V. The difference between the calibration factors measured in those two ways were usually within a 10% margin of experimental error.

Correction of AOD Response. In order to correctly measure the phase of the displacement response with respect to the driving signal, all instruments have to be checked for their own charac-

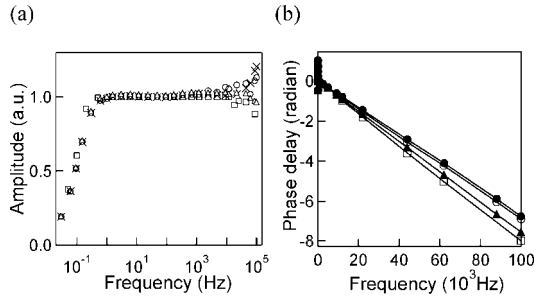

Figure 8. Collection of system responses obtained after repeated optical alignments. Diffraction of the oscillating drive laser by a colloidal particle attached to the glass surface was measured with the QPD. (a) The amplitude of the system response decays at low frequencies due to the ac coupling input into the lock-in amplifier. At high frequencies around 100 kHz, an ambiguity of amplitude is observed within 15%. (b) Phase delay of the system response is linear with the applied frequency. The slope was dependent on the optical alignment (position of laser path in AOD).

teristic response (time delay), which has to be corrected for using the direct output of the lock-in amplifier. Figure 8 shows the response function of our experimental system (amplitude and phase delay) measured by using a probe particle attached to the coverslip and driving the AOD with a signal of constant amplitude and varying frequency from the VCO. Since the particle did not move in response to the oscillation of driving laser, the output of the QPD that detected the probe laser did not give an oscillating response. Instead, the output of the QPD that detected the drive laser was fed into the lock-in amplifier, and amplitude and phase as a function of frequency were recorded. The amplitude of the output of the lock-in amplifier decreased at frequencies lower than 1 Hz because of the ac coupling of the input signal channel (Figure 8a). A significant phase delay therefore also occurred in this regime, which had to be corrected (data not shown). Except at those low frequencies, the phase delay changed linearly with the oscillation frequency (Figure 8b). The reason for this delay is the finite time it takes for the ultrasonic wave generated by a piezo crystal at the edge of the AOD crystal to reach the position where the incident laser beam passes through the crystal. The phase delay ϕ caused by this finite time delay of the ultrasound wave is

$$t = \frac{l}{v} = \frac{\phi}{\omega} \tag{24}$$

where l is the distance the ultrasound wave has to travel and $v \sim 4 \times 10^5$ cm/s is the velocity of ultrasound wave in the AOD crystal (TeO_2). From Figure 8b, we deduce approximately $l \sim 3$ cm, which depends on the alignment of the optics, as shown in Figure 8b, since l is arbitrarily determined. Therefore, the calibration for the response of the experimental system had to be performed before every experiment if the laser alignment had been changed. At very high frequencies, the amplitude of the QPD output varied randomly within the error of ~15%, depending on the alignment of the optics. This is likely to be an artifact that comes from the AOD. At high frequencies ($f \sim 10^5$ Hz), the wavelength of the ultrasound wave (v/f) and the diameter of the driving laser beam in the AOD (~ 1 cm) became comparable so that the laser was not diffracted uniformly, and the profile of the diffracted laser was distorted. Since the distortion of the driving laser is directly detected in the corresponding QPD, the artifact found in Figure 8a is more pronounced than that detected in the response measured with the QPD for the overlapped stationary detection laser. In that case only the force driving the particle is affected, but not the detection by the probe laser. Therefore, the high-frequency error in the amplitude due to a nonuniform laser deflection was at most 15%, which was neglected in this study.

Photothermal Effect. Although water is relatively transparent (absorption length ~10 cm) for the near-infrared red light used for optical trapping ($\lambda = 1064$, 830 nm), the small absorption of the drive laser still resulted in heating of the sample near the laser focus.[54] This sample heating leads to a small refractive index gradient that acts as an effective optical lens,[55] causing deflection of the probe laser. This phenomenon, known as the photothermal lens effect, must be subtracted from the observed signal when its effects are significant. Open squares in Figure 9a show the pure photothermal effect, which was measured with the active method in water in the absence of a probe bead at the focus (situation 3 in Figure 9b). The filled circles show the output of the lock-in amplifier measured in the normal way in water with a probe particle at the laser focus (situation 4).

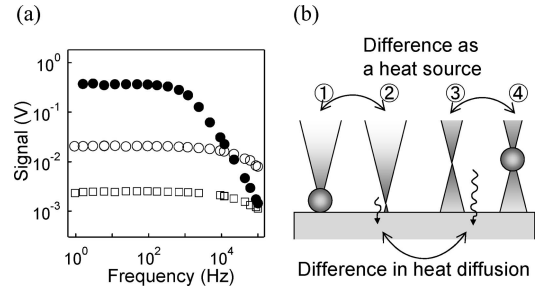

Figure 9. Photothermal effect. (a) QPD response for the probe laser overlapping with the drive laser was detected in the lock-in amplifier without trapping a probe particle in water (open squares) and in glycerol (open circles). The signal level in water measured by the trapping probe particle (filled circles) was larger than the photothermal effect. (b) Schematic illustrating the photothermal lens effect in different conditions.

Laser absorption and the temperature coefficient of the refractive index are both smaller for silica particles than for water. We compared the photothermal effect from a silica particle attached to a coverslip (situation 1) as well as in water (without a trapped particle, situation 2) and found that the photothermal effect for silica particles ($a = 1.28$ μm) was 4−5 times smaller than that of water. The photothermal effect is also dependent on the height of the laser focus above the coverslip because of (i) spherical aberration and (ii) the finite time delay for thermal diffusion from heat source (laser focus) to heat sink (coverslip). The effectiveness of the coverslip as a heat sink has been discussed in detail elsewhere.[54] Therefore, we estimate the photothermal effect from the silica particle trapped 20 μm away from the surface and the photothermal effect in water at the same height while taking a 4−5 times difference in the efficiency of heat absorption between silica and water into consideration. The desired signal, which is purely proportional to the displacement of the probe particle, was obtained by correcting the photothermal effect estimated in this way.

Sample Preparation. Monomeric actin (G-actin) is a globular protein that polymerizes to form semiflexible filaments (F-actin) in buffer with Mg^{2+} and ATP. Actin and myosin II were prepared from rabbit skeletal muscle according to published methods.[56] Actin was stored at −80 °C in G-buffer (2 mM Tris-Cl, 0.2 mM $CaCl_2$, 0.5 mM DTT, 0.2 mM ATP, pH 7.5) and myosin at −80 °C in high salt buffer (0.6 M KCl, 50 mM KH_2PO_4, PH 6.5). To obtain entangled actin solution, actin (3.4 mg/mL) and probe particles are diluted into F-buffer, which contains (HEPES 2 mM, $MgCl_2$ 2 mM, KCl 50 mM, ATP 1 mM, EGTA 1 mM, pH7.2). For active actin−myosin solution, actin and myosin (170 nM) were diluted into F-buffer. After mixing, samples were immediately infused into sample chambers (inner dimensions 15 mm × 3 mm × 100 μm) made from a microscope slide, a coverslip, and double-stick tape. Samples were kept at rest at least for 1 h in order to let them polymerize completely before starting the experiment.

Acknowledgment. We thank K. Vermeulen for sample preparation. This work was supported in part by the Dutch Foundation for Fundamental Research on Matter (FOM). Additional support for C.F.S. and D.M. was provided by the German Science Foundation (DFG) Center for the Molecular Physiology of the Brain (CMPB) and by the DFG Sonderforschungsbereich SFB755. D.M.

was supported by KAKENHI and the Program for Improvement of Research Environment for Young Researchers from Special Coordination Funds for Promoting Science and Technology (SCF), Japan.

References and Notes

(1) Larson, R. G. *The Structure and Rheology of Complex Fluids*; Oxford University Press: New York, 1999.
(2) Mofrad, M. R. K.; Kamm, R. D. *Cytoskeletal Mechanics: Models and Measurements*; Cambridge University Press: New York, 2006.
(3) Kimura, Y.; Mori, T.; Yamamoto, A.; Mizuno, D. *Mol. Cryst. Liq. Cryst.* **2005**, *435*, 711–721.
(4) Mason, T. G.; Weitz, D. A. *Phys. Rev. Lett.* **1995**, *74* (7), 1250–1253.
(5) Gittes, F.; Schnurr, B.; Olmsted, P. D.; MacKintosh, F. C.; Schmidt, C. F. *Phys. Rev. Lett.* **1997**, *79* (17), 3286–3289.
(6) Schnurr, B.; Gittes, F.; MacKintosh, F. C.; Schmidt, C. F. *Macromolecules* **1997**, *30* (25), 7781–7792.
(7) Mason, T. G.; Ganesan, K.; van Zanten, J. H.; Wirtz, D.; Kuo, S. C. *Phys. Rev. Lett.* **1997**, *79* (17), 3282–3285.
(8) Crocker, J. C.; Valentine, M. T.; Weeks, E. R.; Gisler, T.; Kaplan, P. D.; Yodh, A. G.; Weitz, D. A. *Phys. Rev. Lett.* **2000**, *85* (4), 888–891.
(9) Berg-Sorensen, K.; Flyvbjerg, H. *Rev. Sci. Instrum.* **2004**, *75* (3), 594–612.
(10) Peterman, E. J. G.; van Dijk, M. A.; Kapitein, L. C.; Schmidt, C. F. *Rev. Sci. Instrum.* **2003**, *74* (7), 3246–3249.
(11) Dasgupta, B. R.; Weitz, D. A. *Phys. Rev. E* **2005**, *71* (2), 021504.
(12) Ehrenberg, M.; McGrath, J. *Biophys. J.* **2004**, *86* (1), 570a000.
(13) Valentine, M. T.; Perlman, Z. E.; Gardel, M. L.; Shin, J. H.; Matsudaira, P.; Mitchison, T. J.; Weitz, D. A. *Biophys. J.* **2004**, *86* (6), 4004–4014.
(14) Atakhorrami, M.; Koenderink, G. H.; MacKintosh, F. C.; Schmidt, C. F., unpublished.
(15) Levine, A. J.; Lubensky, T. C. *Phys. Rev. Lett.* **2000**, *85* (8), 1774–1777.
(16) Buchanan, M.; Atakhorrami, M.; Palierne, J. F.; Schmidt, C. F. *Macromolecules* **2005**, *38* (21), 8840–8844.
(17) Levine, A. J.; Lubensky, T. C. *Phys Rev E* **2002**, *65* (1), 011501.
(18) Mizuno, D.; Tardin, C.; Schmidt, C. F.; MacKintosh, F. C. *Science* **2007**, *315* (5810), 370–373.
(19) Hough, L. A.; Ou-Yang, H. D. *Phys. Rev. E* **2002**, *65* (2), 021906.
(20) Mizuno, D.; Kimura, Y.; Hayakawa, R. *Phys. Rev. Lett.* **2001**, *8708* (8), 088104.
(21) Amblard, F.; Maggs, A. C.; Yurke, B.; Pargellis, A. N.; Leibler, S. *Phys. Rev. Lett.* **1996**, *77* (21), 4470–4473.
(22) Bausch, A. R.; Ziemann, F.; Boulbitch, A. A.; Jacobson, K.; Sackmann, E. *Biophys. J.* **1998**, *75* (4), 2038–2049.
(23) Ziemann, F.; Radler, J.; Sackmann, E. *Biophys. J.* **1994**, *66* (6), 2210–2216.
(24) Atakhorrami, M.; Kwiecinska, J.; Addas, K. M.; Koenderink, G. H.; Levine, A.; MacKintosh, F. C.; Schmidt, C. F. *Phys. Rev. E* **2006**, *73*, 061501.
(25) Landau, L. D.; Lifshiëtìs, E. M.; Pitaevskiæi, L. P. *Statistical Physics*, 3rd ed.; Butterworth-Heinemann: Oxford, 1980.
(26) Gittes, F.; MacKintosh, F. C. *Phys. Rev. E* **1998**, *58* (2), R1241–R1244.
(27) Atakhorrami, M.; Koenderink, G. H.; Schmidt, C. F.; MacKintosh, F. C. *Phys. Rev. Lett.* **2005**, *95* (20), 208302.
(28) Atakhorrami, M.; Mizuno, D.; Koenderink, G. H.; Liverpool, T. B.; MacKintosh, F. C.; Schmidt, C. F. *Phys. Rev. E* **2008**, *77* (6), 061508.
(29) Bedeaux, D.; Mazur, P. *Physica* **1974**, *78* (3), 505–515.
(30) Bedeaux, D.; Mazur, P. *Physica* **1974**, *76* (2), 247–258.
(31) Liverpool, T. B.; MacKintosh, F. C. *Phys. Rev. Lett.* **2005**, *95* (20), 208303.
(32) Gisler, T.; Weitz, D. A. *Phys. Rev. Lett.* **1999**, *82* (7), 1606–1609.
(33) Morse, D. C. *Macromolecules* **1998**, *31* (20), 7044–7067.
(34) Morse, D. C. *Phys. Rev. E* **1998**, *58* (2), R1237–R1240.
(35) Koenderink, G. H.; Atakhorrami, M.; MacKintosh, F. C.; Schmidt, C. F. *Phys. Rev. Lett.* **2006**, *96* (13), 13807.
(36) Gardel, M. L.; Shin, J. H.; MacKintosh, F. C.; Mahadevan, L.; Matsudaira, P. A.; Weitz, D. A. *Phys. Rev. Lett.* **2004**, *93* (18), 188102.
(37) Everaers, R.; Julicher, F.; Ajdari, A.; Maggs, A. C. *Phys. Rev. Lett.* **1999**, *82* (18), 3717–3720.
(38) Hallatschek, O.; Frey, E.; Kroy, K. *Phys. Rev. Lett.* **2005**, *94* (7), 077804.
(39) Pasquali, M.; Shankar, V.; Morse, D. C. *Phys. Rev. E* **2001**, *6402* (2), 020802.
(40) Watanabe, N.; Mitchison, T. J. *Science* **2002**, *295* (5557), 1083–1086.
(41) Chen, Y. L.; Schweizer, K. S. *J. Phys. Chem. B* **2004**, *108* (21), 6687–6696.
(42) Chen, D. T.; Weeks, E. R.; Crocker, J. C.; Islam, M. F.; Verma, R.; Gruber, J.; Levine, A. J.; Lubensky, T. C.; Yodh, A. G. *Phys. Rev. Lett.* **2003**, *90* (10), 108301.
(43) Huh, J. Y.; Furst, E. M. *Phys. Rev. E* **2006**, *74* (3), 031802.
(44) de Gennes, P.-G. *Scaling Concepts in Polymer Physics*; Cornell University Press: Ithaca, NY, 1979; p 324.
(45) Moore, M. A. *J. Phys. A: Math. Gen.* **1977**, *10* (2), 305–314.
(46) Lau, A. W. C.; Hoffman, B. D.; Davies, A.; Crocker, J. C.; Lubensky, T. C. *Phys. Rev. Lett.* **2003**, *91* (19), 198101.
(47) Crocker, J. C.; Hoffman, B. D. *Cell Mech.* **2007**, *83*, 141–178.
(48) MacKintosh, F. C.; Levine, A. J. *Phys. Rev. Lett.* **2008**, *1* (1), 018104.
(49) Humphrey, D.; Duggan, C.; Saha, D.; Smith, D.; Kas, J. *Nature (London)* **2002**, *416* (6879), 413–416.
(50) Gittes, F.; Schmidt, C. F. *Opt. Lett.* **1998**, *23* (1), 7–9.
(51) Gittes, F.; Schmidt, C. F. *Methods Cell Biol.* **1998**, *55*, 129–156.
(52) Vermeulen, K. C.; Wuite, G. J. L.; Stienen, G. J. M.; Schmidt, C. F. *Appl. Opt.* **2006**, *45* (8), 1812–1819.
(53) Zemanek, P.; Jonas, A.; Sramek, L.; Liska, M. *Opt. Commun.* **1998**, *151* (4−6), 273–285.
(54) Peterman, E. J. G.; Gittes, F.; Schmidt, C. F. *Biophys. J.* **2003**, *84* (2), 1308–1316.
(55) Cognet, L.; Tardin, C.; Boyer, D.; Choquet, D.; Tamarat, P.; Lounis, B. *Proc. Natl. Acad. Sci. U.S.A.* **2003**, *100* (20), 11350–11355.
(56) Cunningham, L. W.; Frederiksen, D. W.; Vallee, R. B. *Structural and Contractile Proteins*; Academic Press: New York, 1982.

MA801218Z